EPJ B
Condensed Matter and Complex Systems
EPJ.org your physics journal

Eur. Phys. J. B (2017) 90: 256 DOI: 10.1140/epjb/e2017-80383-1

# Advances in theoretical and experimental XAFS studies of thermodynamic properties, anharmonic effects and structural determination of fcc crystals

Nguyen Van Hung, Cu Sy Thang, Nguyen Ba Duc, Dinh Quoc Vuong, and Tong Sy Tien

edp sciences
Società Italiana di Fisica
Springer

Eur. Phys. J. B (2017) 90: 256
DOI: 10.1140/epjb/e2017-80383-1

THE EUROPEAN PHYSICAL JOURNAL B

Regular Article

# Advances in theoretical and experimental XAFS studies of thermodynamic properties, anharmonic effects and structural determination of fcc crystals

Nguyen Van Hung[1,a], Cu Sy Thang[2,3], Nguyen Ba Duc[4], Dinh Quoc Vuong[5], and Tong Sy Tien[6]

[1] Institute of Research and Development, Duy Tan University, 03 Quang Trung, Da Nang, Viet Nam
[2] Institute of Geological Sciences (IGS), Vietnam Academy of Science and Technology (VAST), 18 Hoang Quoc Viet, Cau Giay, Ha Noi, Viet Nam
[3] Graduate University of Science and Technology, Vietnam Academy of Science and Technology (VAST), 18 Hoang Quoc Viet, Cau Giay, Ha Noi, Viet Nam
[4] Department of Physics, Tan Trao University, Km 6, Trung Mon, Yen Son, Tuyen Quang, Viet Nam
[5] Cam pha School, Quang Ninh Education & Training Department, Nguyen Van Cu, Ha Long, Quang Ninh, Viet Nam
[6] Department of Basic Sciences, University of Fighting & Prevention, 243 Khuat Duy Tien, Thanh Xuan, Ha Noi, Viet Nam

Received 28 June 2017 / Received in final form 8 October 2017
Published online 18 December 2017 – 

**Abstract.** Thermodynamic properties, anharmonic effects and structural determination of fcc crystals have been studied based on the theoretical and experimental Debye–Waller factors presented in terms of cumulant expansion up to the third order, thermal expansion coefficient, X-ray absorption fine structure (XAFS) spectra and their Fourier transform magnitudes. The advances in these studies are performed by the further development of the anharmonic correlated Einstein model primary only for approximating three first XAFS cumulants into the method using that all the considered theoretical and experimental XAFS parameters have been provided based on only the calculated and measured second cumulants. The obtained cumulants describe the anharmonic effects in XAFS contributing to the accurate structural determination. Numerical results for Cu are found to be in good agreement with the experimental values extracted by using the present advanced method and with those obtained by the other measurements.

## 1 Introduction

X-ray Absorption Fine Structure (XAFS) has developed into a powerful technique for providing information on the local atomic structure and thermodynamic properties of substances. The formalism for including anharmonic effects in XAFS is often based on cumulant expansion approach [1] from which the anharmonic XAFS function has resulted as

$$\chi(k) = F(k)\frac{e^{-2R/\lambda(k)}}{kR^2}\mathrm{Im}\left\{e^{i\Phi(k)} \times \exp\left[2ikR + \sum_n \frac{(2ik)^n}{n!}\sigma^{(n)}\right]\right\}, \quad (1)$$

where $F(k)$ is the real atomic backscattering amplitude, $k$ and $\lambda$ are the wave number and mean free path of photoelectron, respectively, $\Phi$ is the net phase shift, $R = \langle r \rangle$ with $r$ being the instantaneous bond length between absorber and backscatterer atoms, and $\sigma^{(n)}(n = 1, 2, 3, \dots)$ are the cumulants describing Debye–Waller factors (DWFs).

Hence, the cumulants or DWFs are very important for the anharmonic XAFS where the even cumulants contribute to the amplitude, the odd ones to the phase of XAFS spectra, and for small anharmonicities, it is sufficient to keep the third and fourth cumulant terms [2]. They are crucial to quantitative treatment of XAFS spectra. Consequently, the lack of the precise DWFs or cumulants has been one of the biggest limitations to accurate structural determinations (e.g., the coordination numbers and the atomic distances) [3] and to specify the thermodynamic properties of substances [4–9] from XAFS experiments. Therefore, investigation of DWFs or cumulants and XAFS is of great interest.

Many efforts have been made to overcome such limitations by the theoretical and experimental investigations, for example see [1–27]. Here the anharmonic correlated Einstein model (ACEM) [10] is successfully applied to XAFS studies but it is limited only for approximating

[a] e-mail: hungnv@vnu.edu.vn

three first XAFS cumulants. Moreover, there is still no method which can provide certain simplification and reduction of XAFS calculations and measurements based on only the leading parameter like the second cumulant.

The purpose of this work is to study the thermodynamic properties, anharmonic effects and structural determination of fcc crystals based on their theoretical and experimental XAFS parameters such as the DWFs presented in terms of cumulant expansion up to the third order, thermal expansion coefficient, XAFS spectra and their Fourier transform magnitudes. The advances in these studies are performed by the further development of the ACEM [10] into the present method applied not only to theoretical but also to experimental XAFS studies based on that the XAFS calculations and measurements are necessary only for the second cumulants from which all the considered XAFS parameters can be provided. This method has resulted (Sect. 2) based on describing the quantum statistically derived analytical expressions of all the considered XAFS quantities in terms of second cumulants or mean square relative displacements (MSRDs). The many-body effects included in the present one-dimensional model have been taken into account based on the first shell near neighbor contributions approach (FSNNA) to the vibrations between absorber and backscatter atoms. Morse potential is assumed to describe the single-pair atomic interaction included in the anharmonic interatomic effective potential. The obtained cumulants describing anharmonic effects in XAFS contribute to the accurate structural determination. Numerical results for Cu in fcc phase (Sect. 3) are compared to the experimental values measured at the Beamline BL8, Synchrotron Light Research Institute (SLRI), Thailand, at 300 K, 400 K, 500 K and to those obtained by the other measurements [11–14]. They show their good agreement and the evident temperature dependence of the thermodynamic properties, anharmonic effects and structural parameters of the considered material. The conclusions on the obtained results are presented in Section 4.

## 2 Advanced method for XAFS calculations and measurements

### 2.1 XAFS cumulants and thermal expansion coefficient of fcc crystals

In order to include anharmonic effects, the Hamiltonian of system in the present theory involves the anharmonic interatomic effective potential expanded up to the third order as

$$V_{eff}(x) \approx \frac{1}{2}k_{eff}x^2 + k_{3eff}x^3, \quad x = r - r_0, \tag{2}$$

where $k_{eff}$ is the effective local force constant and $k_{3eff}$ is the cubic anharmonic parameter giving an asymmetry of the anharmonic effective potential, $r$ and $r_0$ are the instantaneous and equilibrium distances between absorber and backscatterer atoms, respectively.

The values of $k_{eff}$, $k_{3eff}$ for fcc crystals included in all cumulants and XAFS expressions are determined based on the FNNCA which was successfully applied to bcc crystals [9]. For fcc structure, each atom is bonded to its 12 first shell near neighbors, so that the oscillation of a single bond pair of atoms (e.g., absorber and backscatterer) is influenced by their first shell near neighbors. Therefore, the anharmonic interatomic effective potential equation (2) has the form

$$\begin{aligned} V_{eff}(x) &= V(x) + \Psi(x), \\ \Psi(x) &= 2V\left(-\frac{x}{2}\right) + 8V\left(-\frac{x}{4}\right) + 8V\left(\frac{x}{4}\right), \end{aligned} \tag{3}$$

which is the sum over not only the term $V(x)$ describing the pair-interaction between absorber and backscatterer atoms but also the second one $\Psi(x)$ including the contributions of projections of pair-interactions of absorber and bacscatterer with their first shell near neighbors along the bond direction. Unfortunately, in equation (3) $\Psi(x)$ contains only 18 terms because the contributions of two first shell near neighbors being the absorber and backscatterer are already included in $V(x)$ and those of 4 others lying in the surface perpendicular to the bond direction provide zero contribution.

Hence, in equation (3) by including the first shell near neighbors contributions to the vibration between absorber and backscatterer atoms the many-body effects or an affect of crystal lattice on atomic vibration have been taken into account, and by projecting such contributions along the bond direction the purely one-dimensional model is recovered. This is the significance of the anharmonic effective potential for XAFS study in the present many-body fcc system.

The Morse potential expanded up to the third order around its minimum

$$\begin{aligned} V(x) &= D\left(e^{-2\alpha x} - 2e^{-\alpha x}\right) \\ &\approx D\left(-1 + \alpha^2 x^2 - \alpha^3 x^3\right), \end{aligned} \tag{4}$$

is assumed to describe the single-pair atomic interaction included in the anharmonic effective potential given by equation (3) where $\alpha$ describes the width of the potential and $D$ is the dissociation energy.

For deriving XAFS cumulants we describe the anharmonic interatomic effective potential equation (3) for fcc crystals in the summation of the harmonic contribution and a perturbation $\delta V$ due to anharmonicity in XAFS as

$$\begin{aligned} V_{eff}(y) &= \frac{1}{2}k_{eff}y^2 + \delta V(y), \\ \delta V &\cong 5D\alpha^2 a y + k_{3eff}y^3, \quad y = x - a, \; a = \langle x \rangle. \end{aligned} \tag{5}$$

The derivation of XAFS cumulants for fcc crystals in this work is based on quantum statistical perturbation theory [28] and the parameters of the anharmonic interatomic effective potentials given by equations (2), (3) and (5),

as well as an averaging procedure using the canonical partition function $Z$ and statistical density matrix $\rho$, e.g.,

$$\langle y^m \rangle = \frac{1}{Z} Tr\left(\rho\, y^m\right), \quad m = 1, 2, 3, \ldots \tag{6}$$

Atomic vibrations are quantized in terms of phonons, and anharmonicity is the result of phonon–phonon interaction, that is why we express $y$ in terms of the annihilation and creation operators, $\hat{a}$ and $\hat{a}^+$, respectively

$$y \equiv a_0\left(\hat{a} + \hat{a}^+\right), \quad a_0 = \sqrt{\frac{\hbar\omega_E}{10D\alpha^2}}, \tag{7}$$

which have the following properties

$$\begin{aligned} \hat{a}^+|n\rangle &= \sqrt{n+1}|n+1\rangle, \\ \hat{a}|n\rangle &= \sqrt{n-1}|n-1\rangle, \\ \hat{a}^+\hat{a}|n\rangle &= n|n\rangle, \\ \left[\hat{a}, \hat{a}^+\right] &= 1, \end{aligned} \tag{8}$$

as well as use the harmonic oscillator state $|n\rangle$ as the eigenstate with the eigenvalue $E_n = n\hbar\omega_E$ for $n$ being the phonon number, ignoring the zero-point energy for convenience.

The operations expressed by equation (8) have been applied to calculate the matrix elements for deriving the cumulants using the procedure depicted by equations (6) and (7).

Consequently, the analytical XAFS expressions have resulted for the second cumulant or MSRD

$$\begin{aligned} \sigma^2(T) &= \sigma_0^2 \frac{1+z(T)}{1-z(T)}, \\ \sigma_0^2 &= \frac{\hbar\omega_E}{10D\alpha^2}, \\ z(T) &= \exp\left(-\theta_E/T\right), \end{aligned} \tag{9}$$

for the first cumulant or net thermal expansion

$$\begin{aligned} \sigma^{(1)}(T) &= a = \sigma_0^{(1)} \frac{1+z(T)}{1-z(T)} = \frac{\sigma_0^{(1)}}{\sigma_0^2}\sigma^2(T), \\ \sigma_0^{(1)} &= \frac{3\alpha}{4}\sigma_0^2, \end{aligned} \tag{10}$$

and for the third cumulant or mean cubic relative displacement (MCRD)

$$\begin{aligned} \sigma^{(3)}(T) &= \sigma_0^{(3)}\left[3\left(\frac{\sigma^2(T)}{\sigma_0^2}\right)^2 - 2\right], \\ \sigma_0^{(3)} &= \frac{\alpha}{2}\left(\sigma_0^2\right)^2, \end{aligned} \tag{11}$$

where the correlated Einstein frequency and temperature contained in the above cumulants are given by

$$\omega_E = \sqrt{\frac{10D\alpha^2}{M}}, \quad \theta_E = \frac{\hbar\omega_E}{k_B}, \tag{12}$$

$M$ is the atomic mass and $k_B$ is Boltzmann constant.

Moreover, using the first cumulant given by equation (10), the expression for thermal expansion coefficient has been derived and given by

$$\begin{aligned} \alpha_T(T) &= \frac{1}{r}\frac{da}{dT} = \alpha_T^0 \frac{\left(\sigma^2(T)\right)^2 - \left(\sigma_0^2\right)^2}{T^2}, \\ \alpha_T^0 &= \frac{15D\alpha^3}{4k_B r}. \end{aligned} \tag{13}$$

In the above obtained expressions, $\sigma_0^{(1)}$, $\sigma_0^2$, $\sigma_0^{(3)}$ are zero-point energy contributions to three first XAFS cumulants $\sigma^{(1)}(T)$, $\sigma^2(T)$, $\sigma^{(3)}(T)$, respectively, and $\alpha_T^0$ is the constant value which the thermal expansion coefficient approaches at high-temperatures.

Note that the second cumulant given by equation (9) is harmonic while the experimental data always include the temperature-dependent anharmonic effects. That is why we introduce the total second cumulant or MSRD as

$$\sigma_{tot}^2(T) = \sigma^2(T) + \sigma_A^2(T), \tag{14}$$

which involves an anharmonic contribution

$$\sigma_A^2(T) = \beta_A(T)\left[\sigma^2(T) - \sigma_0^2\right], \tag{15}$$

containing the anharmonic factor

$$\begin{aligned} \beta_A(T) = {} & \frac{9\alpha^2}{8}\sigma^2(T) \\ & \times \left[1 + \frac{3\alpha}{4R}\sigma^2(T)\left(1 + \frac{3\alpha}{4R}\sigma^2(T)\right)\right], \end{aligned} \tag{16}$$

derived based on the relative volume change due to thermal expansion and described also in terms of second cumulant.

Hence, the above derived analytical expressions for the first, third cumulants and thermal expansion coefficient $\sigma^{(1)}$, $\sigma^{(3)}$ and $\alpha_T$, respectively, as well as the total second cumulant given by equations (14)–(16) including anharmonic effects are presented in terms of second cumulant $\sigma^2$ or MSRD. This leads to creating the present advanced method based on that the calculations and measurements are necessary only for the second cumulants from which the first, third cumulants, thermal expansion coefficient and other XAFS parameters can be provided.

### 2.2 Anharmonic XAFS based on cumulant expansion

For anharmonic XAFS calculation, we develop further the XAFS function given by equation (1) into an analytical form explicitly including the above obtained cumulants for the temperature-dependent K-edge anharmonic XAFS spectra as

$$\chi(k,T) = \sum_j \frac{S_0^2 N_j}{kR_j^2} F_j(k) F_A(k,T) e^{-\left(2k^2\sigma^2(T) + 2R_j/\lambda(k)\right)} \times \sin\left(2kR_j + \Phi_j(k) + \Phi_A^j(k,T)\right), \quad (17)$$

which contains the anharmonic contribution to amplitude described by the factor

$$F_A(k,T) = \exp\left[-2k^2\sigma_A^2(T)\right], \quad (18)$$

causing the anharmonic attenuation and the anharmonic contribution to phase

$$\Phi_A^j(k,T) = 2k\left[\sigma^{(1)}(T) - 2\sigma_A^2(T)\left(\frac{1}{R_j} - \frac{1}{\lambda(k)}\right) - \frac{2}{3}\sigma^{(3)}(T)k^2\right], \quad (19)$$

causing the anharmonic phase shift of XAFS spectra. Here, the derivation of equation (19) is based on equation (5) of reference [2] applied to the present case.

In the anharmonic XAFS function given by equation (17), $S_0^2$ is the square of the many body overlap term, $N_j$ is the atomic number of each shell, the second cumulant $\sigma^2$ and its anharmonic contribution $\sigma_A^2$ are calculated by equations (9) and (15), respectively, the mean free path $\lambda$ is defined by the imaginary part of the complex photoelectron momentum $p = k + i/\lambda$, and the sum $j$ is over all the considered atomic shells. Moreover, all parameters of this function can be obtained from the second cumulants or MSRDs, and this function equation (17) will return to the harmonic case calculated by the well-known FEFF code [29] if the anharmonic contributions to amplitude $F_A(k,T)$ and to phase $\Phi_A(k,T)$ are excluded. Inversely, the FEFF code can also be modified by including these anharmonic contributions to XAFS amplitude and phase to calculate the anharmonic XAFS spectra and their Fourier transform magnitudes. This is the evident advantage of the present advanced method which will be applied to the numerical calculations of the considered XAFS quantities and to the extraction of experimental data for Cu presented in Section 3.

## 3 Experimental and numerical results and discussions

### 3.1 Experimental

The measurements of second cumulants or MSRDs, XAFS spectra and their Fourier transform magnitudes of Cu in fcc phase at 300 K, 400 K and 500 K have been performed at the Beamline BL8 (SLRI, Thailand). It is the routinely operated for X-ray absorption spectroscopy (XAS) in an immediate photon energy range (1.25–10 keV). The experimental set-up conveniently facilitates XAS measurements in transmission and fluorescence-yield modes at several K-edges of elements ranging from magnesium to zinc [30]. The experimental values of the first, third cumulants, thermal expansion coefficients and other XAFS parameters of Cu at 300 K, 400 K, and 500 K have been extracted from the measured values of second cumulants using the present advanced method based on the description of these quantities in terms of second cumulants presented in Section 2. The obtained experimental values will be presented in Section 3.2 compared to the calculated results and to those measured by the other works [11–14].

### 3.2 Numerical results compared to experiment and discussions

Now the expressions derived in the previous Section 2 are applied to numerical calculations for Cu using its Morse potential parameters [31] $D = 0.3429$ eV, $\alpha = 1.3588$ Å$^{-1}$ which were obtained using experimental values for the energy of sublimation, the compressibility, and the lattice constant.

#### 3.2.1 XAFS cumulants and thermal expansion coefficient

Figure 1 illustrates good agreement of (a) first cumulant $\sigma^{(1)}(T)$ and (b) total and harmonic second cumulants $\sigma_{tot}^2(T)$, $\sigma^2(T)$, respectively, of Cu calculated using the present theory with the experimental values at 300 K, 400 K and 500 K extracted by using the present advanced method and with the other measured data [11] for the first cumulant and [12] for the second cumulant. Here, $\sigma_{tot}^2(T)$ is a little different from $\sigma^2(T)$ at temperatures greater than the room temperature due to the anharmonic contributions. Note that from this first cumulant we can also obtain temperature dependence of the first shell near neighbor distance based on the expression $R(T) = R(0) + \sigma^{(1)}(T)$.

Temperature dependence of third cumulant $\sigma^{(3)}(T)$ (Fig. 2a) and thermal expansion coefficient $\alpha_T(T)$ (Fig. 2b) of Cu calculated using the present theory agrees well with the experimental values at 300 K, 400 K and 500 K extracted by using the present advanced method and with the other measured data [12,13] for the third cumulant and [14] for the thermal expansion coefficient. Here, the theoretical and experimental thermal expansion coefficients of Cu approach the constant values at high-temperatures.

Figure 3 illustrates good agreement of temperature dependence of (a) anharmonic contributions $\sigma_A^2(T)$ to the

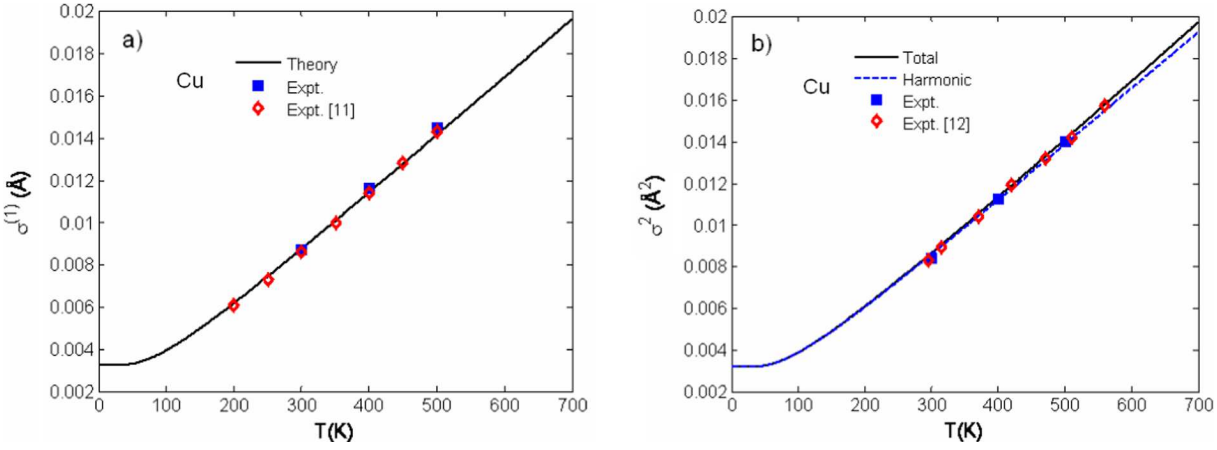


**Fig. 1.** Temperature dependence of (a) first cumulant $\sigma^{(1)}(T)$ and (b) total and harmonic second cumulants $\sigma^2_{tot}(T)$ and $\sigma^2(T)$, respectively, of Cu calculated using the present theory compared to the experimental values at 300 K, 400 K, 500 K measured in this work and with the other measured values [11] for the first cumulant and [12] for the second cumulant.

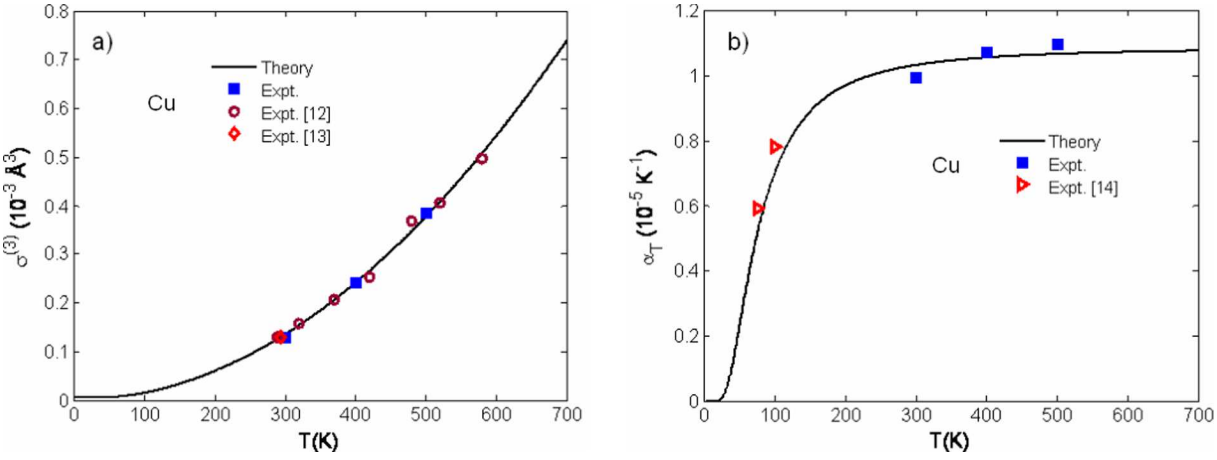


**Fig. 2.** Temperature dependence of (a) third cumulant $\sigma^{(3)}(T)$ and (b) thermal expansion coefficient $\alpha_T(T)$ of Cu calculated using the present theory compared to the experimental values at 300 K, 400 K, 500 K extracted by using the present advanced method and with the other measured data [12,13] for the third cumulant and [14] for the thermal expansion coefficient.

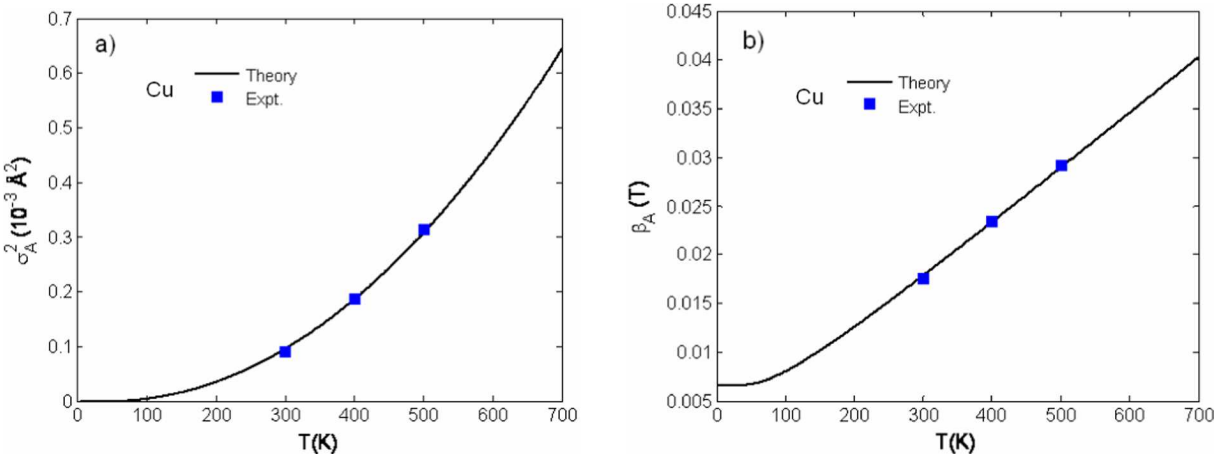


**Fig. 3.** Temperature dependence of (a) anharmonic contribution $\sigma^2_A(T)$ to second cumulant or MSRD and (b) anharmonic factor $\beta_A(T)$ of Cu calculated using the present theory compared to the experimental values at 300 K, 400 K and 500 K extracted by using the present advanced method.

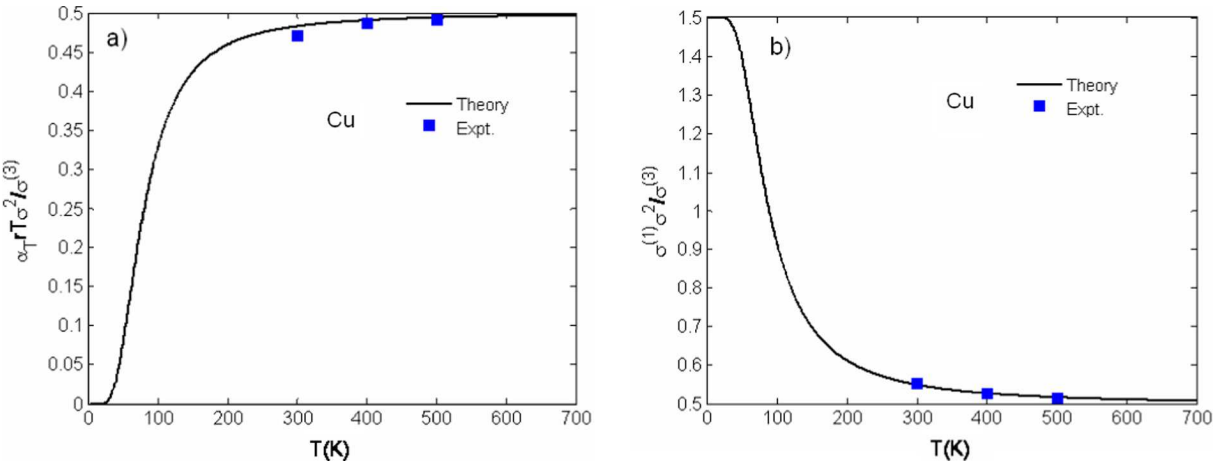


**Fig. 4.** Temperature dependence of cumulant ratios (a) $\alpha_T r T\sigma^2/\sigma^{(3)}$ and (b) $\sigma^{(1)}\sigma^2/\sigma^{(3)}$ of Cu calculated using the present theory compared to the experimental values at 300 K, 400 K and 500 K.

second cumulant or MSRD and (b) anharmonic factor $\beta_A(T)$ characterizing percentage of anharmonic contributions at each temperature of Cu calculated using the present theory with their experimental values at 300 K, 400 K and 500 K extracted by using the present advanced method. These values are normally difficult to be directly measured, but using the present advanced method they have been calculated and extracted from the calculated and measured second cumulants.

The cumulant ratios $\alpha_T r T\sigma^2/\sigma^{(3)}$ and $\sigma^{(1)}\sigma^2/\sigma^{(3)}$ are often considered as the standards for cumulant studies [8–10,15] and to identify the temperature above which the classical limit is applicable [10]. Figure 4 shows good agreement of temperature dependence of (a) $\alpha_T r T\sigma^2/\sigma^{(3)}$ and (b) $\sigma^{(1)}\sigma^2/\sigma^{(3)}$ of Cu calculated using the present theory with the experimental values at 300 K, 400 K and 500 K extracted by using the present advanced method. The theoretical and experimental results of these ratios show that above the Einstein temperature ($\theta_E = 218$ K calculated using the present theory for Cu) they approach the classical value of 1/2 [8,15] so that the classical limit is applicable.

Consequently, the thermodynamic properties and anharmonic effects of Cu in fcc phase have been studied based on the anharmonic XAFS parameters. Here, the second cumulant describing MSRD is primary a harmonic effect plus small anharmonic contributions which appear only at high-temperatures. But the first cumulant describing the net thermal expansion or lattice disorder, the third cumulant or MCRD describing the asymmetry of pair atomic distribution function and the thermal expansion coefficient are entirely anharmonic effects. The good agreement of the theoretical and experimental values of the above quantities calculated and extracted by using the present advanced method with the measured data of the other works [11–14] denotes not only the efficiencies of this advanced method but also its better advantages described by the simplification and reduction of XAFS calculations and measurements shown by obtaining all the considered theoretical and experimental XAFS quantities only from the calculated and measured second cumulants.

### 3.2.2 XAFS spectra and their Fourier transform magnitudes

In XAFS technique, XAFS spectra and their Fourier transform magnitudes provide structural information of substances [1]. Based on the present advanced method, the FEFF code [29] has been modified by using equation (17) including the amharmonic contributions to XAFS amplitude (Eq. (18)) and phase (Eq. (19)) described by the above obtained cumulants to calculate XAFS spectra at 300 K, 400 K and 500 K of Cu and their Fourier transform magnitudes.

Figure 5 illustrates (a) the anharmonic amplitude attenuation factor $F_A(k,T)$ and (b) the phase shift $\Phi_A(k,T)$ of XAFS of Cu at 300 K, 400 K and 500 K calculated using the present theory based on the above obtained cumulants. The increase of these values shows the increase of anharmonicity as the wave number $k$-value and temperature $T$ increase.

Using the obtained $F_A(k,T)$ and $\Phi_A(k,T)$ (Fig. 5), the anharmonic XAFS spectra of Cu at 300 K, 400 K and 500 K have been calculated and presented in Figure 6a compared to their measured results presented in Figure 6b. The anharmonic amplitude attenuation and phase shift are evidently shown in both the theoretical and experimental XAFS spectra. These theoretical and experimental anharmonic XAFS spectra have been Fourier transformed and their Fourier transform magnitudes are presented in Figure 7. They show good agreement between the theoretical and experimental results, as well as the decrease of the peak heights and their shifts to the left as the temperature $T$ increases.

Note that the anharmonic XAFS spectra of Cu at 300 K, 400 K, 500 K (Fig. 6a) and their Fourier transform magnitudes (Fig. 7) calculated based on including the anharmonic contributions to XAFS amplitude and phase using the cumulants obtained from the second cumulants or MSRDs are found to be in good agreement with the measured data. Moreover, using the present advanced method and the measured second cumulants of Cu at 300 K, 400 K and 500 K we have reproduced all the considered experimental values including XAFS spectra

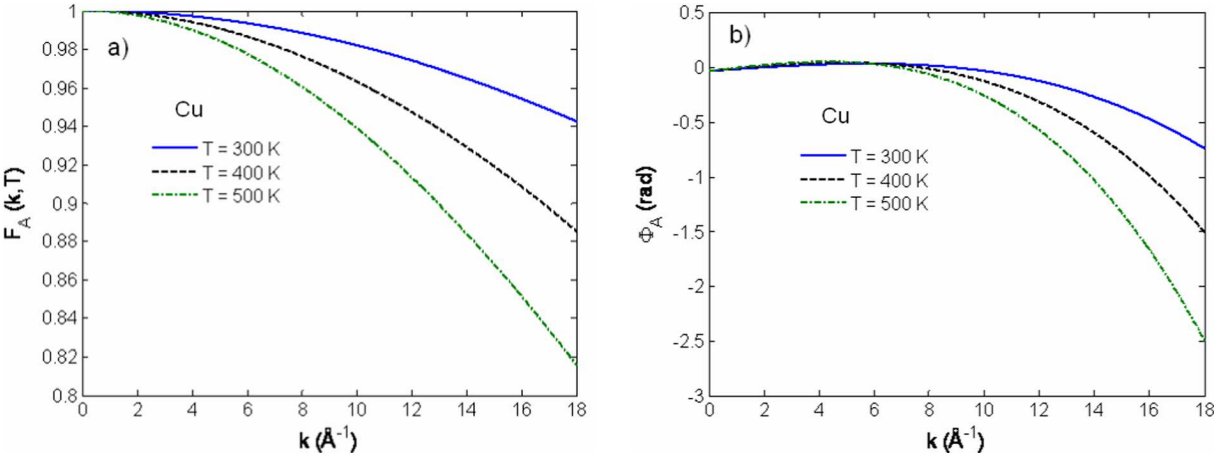


**Fig. 5.** Wave number k-dependence of (a) anharmonic amplitude attenuation factor $F_A(k,T)$ and (b) phase shift $\Phi_A(k,T)$ of XAFS of Cu at 300 K, 400 K and 500 K calculated using the present theory.

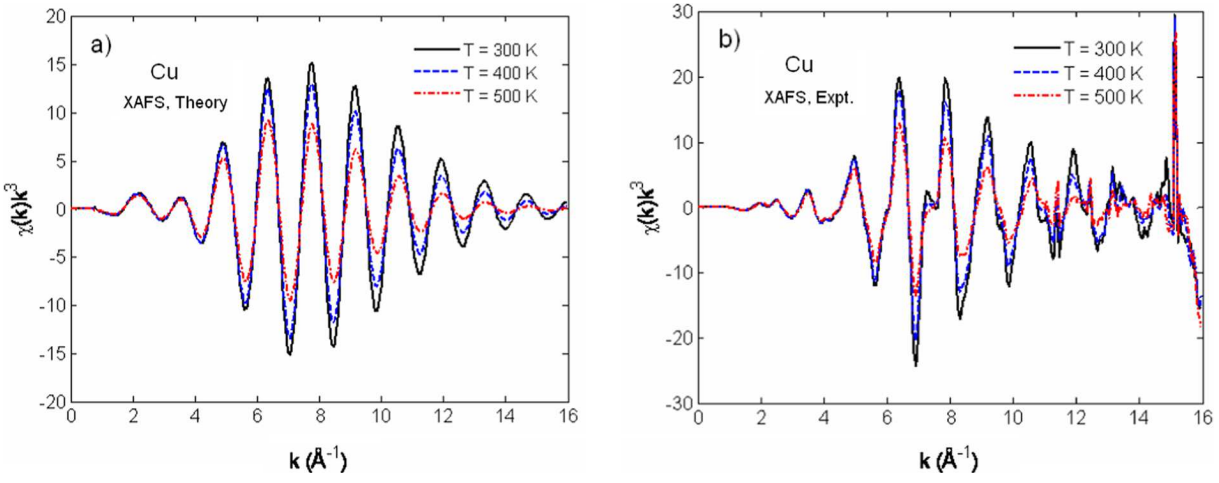


**Fig. 6.** (a) Theoretical XAFS spectra of Cu at 300 K, 400 K and 500 K calculated using the present theory and (b) their experimental results measured at the Beamline BL8 (SLRI, Thailand).

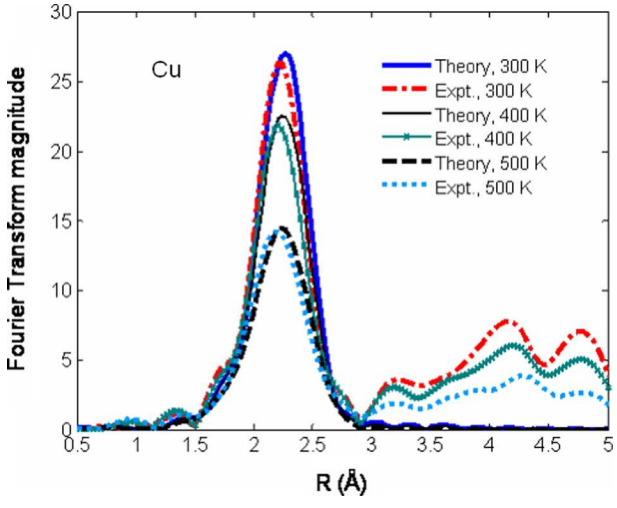


**Fig. 7.** Comparison of Fourier transform magnitudes of theoretical XAFS spectra of Cu at 300 K, 400 K and 500 K (Fig. 6a) with those of their experimental results (Fig. 6b).

and their Fourier transform magnitudes. The obtained results agree well with the experimental values at these temperatures presented in the above figures. That illustrates not only the validity and efficiency of the present advanced method but also its useful contributions to the accurate theoretical and experimental structural determination of the considered crystals based on only the calculated and measured second cumulants or MSRDs.

## 4 Conclusions

In this work, the advances in the theoretical and experimental studies of the thermodynamic properties, anharmonic effects and structural determination of fcc crystals have been performed based on their theoretical and experimental XAFS quantities such as the DWFs presented in terms of cumulant expansion up to the third order, thermal expansion coefficient, XAFS spectra and their Fourier transform magnitudes.

The most advantageous improvement in the above studies has been achieved by the further development of the ACEM primary only for approximating three first XAFS cumulants into the present advanced method applied not only to theoretical but also to experimental XAFS studies using that all the considered theoretical and experimental XAFS quantities including XAFS spectra and their Fourier transform magnitudes, as well as those which are difficult to be directly measured have been provided based on only the calculated and measured second cumulants or MSRDs.

The obtained temperature-dependent theoretical and experimental XAFS quantities have been in detail analyzed and valuated. They include the evident anharmonic effects and satisfy all their fundamental properties, as well as approach the classical values at high-temperatures and contain zero-point energy contributions at low-temperatures, a quantum effect. The obtained theoretical and experimental cumulants describe the anharmonic effects in XAFS spectra and their Fourier transform magnitudes leading to the accurate structural determination of the considered material.

The good agreement between the theoretical and experimental results of XAFS quantities of Cu calculated and extracted by using the present advanced method, as well as their good agreement with the measured data of the other works denotes not only the efficiencies of this advanced method but also its better advantages shown by the above mentioned simplification and reduction of XAFS calculations and measurements based on only the second cumulants or MSRDs. All these results illustrate the simplicity and efficiency of the advances performed in this work in XAFS data analysis and in materials studies.

The authors thank Prof. J.J. Rehr and Prof. P. Fornasini for useful comments. One of the authors (C.S.T.) thanks Dr. Wantana Klysubun, the head of Beamline BL8, and the Synchrotron Light Research Institute (Thailand) for hospitality and assistance during his stay there to perform the necessary measurements. This research is funded by the Vietnam National Foundation for Science and Technology Development (NAFOSTED) under grant number 103.01-2015.10.

## Author contribution statement

We state that all authors contributed to the results of this work where the revisions related to the comments of reviewers have been performed by the corresponding author Nguyen Van Hung.

## References

1. E.D. Crozier, J.J. Rehr, R. Ingalls, in *X-ray absorption*, edited by D.C. Koningsberger, R. Prins (Wiley, New York, 1988), Chap. 9
2. J.M. Tranquada, R. Ingalls, Phys. Rev. B **28**, 3520 (1983)
3. F.D. Vila, J.J. Rehr, H.H. Rossner, H.J. Krappe, Phys. Rev. B **76**, 014301 (2007)
4. N.V. Hung, N.B. Trung, B. Kirchner, Physica B **405**, 2519 (2010)
5. N.V. Hung, V.V. Hung, H.K. Hieu, R.R. Frahm, Physica B **406**, 456 (2011)
6. N.V. Hung, C.S. Thang, N.C. Toan, H.K. Hieu, Vacuum **101**, 63 (2014)
7. N.V. Hung, J. Phys. Soc. Jpn. **83**, 024802 (2014)
8. N.V. Hung, T.S. Tien, N.B. Duc, D.Q. Vuong, Mod. Phys. Lett. B **28**, 1450174 (2014)
9. N.V. Hung, T.T. Hue, H.D. Khoa, D.Q. Vuong, Physica B **503**, 174 (2016)
10. N.V. Hung, J.J. Rehr, Phys. Rev. B **56**, 43 (1997)
11. S.A. Beccara, G. Dalba, P. Fornasini, R. Grisenti, F. Pederiva, A. Sanson, Phys. Rev. B **68**, 140301(R) (2003)
12. V. Pirog, T.I. Nedoseikina, A.I. Zarubin, A.T. Shuvaev, J. Phys.: Condens. Matter **14**, 1825 (2002)
13. T. Yokoyama, T. Sasukawa, T. Ohta, Jpn. J. Appl. Phys. **28**, 1905 (1989)
14. Y.S. Toukian, R.K. Kirby, R.E. Taylor, P.D. Desai, *Thermophysical properties of matter* (IFI/Plenum, New York, 1975)
15. E.A. Stern, P. Livins, Z. Zhang, Phys. Rev. B **43**, 8850 (1991)
16. L. Tröger, T. Yokoyama, D. Arvanitis, T. Lederer, M. Tischer, K. Baberschke, Phys. Rev. B **49**, 888 (1994)
17. A.I. Frenkel, J.J. Rehr, Phys. Rev. B **48**, 585 (1993)
18. T. Miyanaga, T. Fujikawa, J. Phys. Soc. Jpn. **63**, 1036 (1994)
19. T. Yokoyama, Phys. Rev. B **57**, 3423 (1998)
20. A.V. Poiarkova, J.J. Rehr, Phys. Rev. B **59**, 948 (1999)
21. G. Dalba, P. Fornasini, R. Grisenti, J. Purans, Phys. Rev. Lett. **82**, 4240 (1999)
22. I.V. Pirog, T.I. Nedoseikina, Physica B **334**, 123 (2003)
23. J.J. Rehr, J.J. Kas, M.P. Prange, A.P. Sorini, Y. Takimoto, F. Villa, C. R. Phys. **10**, 548 (2009)
24. P. Fornasini, R. Grisenti, J. Synchrotron Rad. **22**, 1242 (2015)
25. N.V. Hung, R. Frahm, Physica B **208**, 91 (1995)
26. N.V. Hung, R. Frahm, H. Kamitsubo, J. Phys. Soc. Jpn. **65**, 3571 (1996)
27. N.V. Hung, J. Phys. IV France **7**, C2 (1997)
28. R.P. Feynman, in *Statistical mechanics*, edited by J. Shaham (W. A. Benjamin, Inc., Advanced Book Program, Reading, MA, 1972)
29. J.J. Rehr, J. Mustre de Leon, S.I. Zabinsky, R.C. Albers, J. Am. Chem. Soc. **113**, 5135 (1991)
30. W. Klysubun, P. Sombunchoo, W. Deenam, C. Komark, J. Synchrotron Rad. **19**, 930 (2012)
31. L.A. Girifalco, W.G. Weizer, Phys. Rev. **114**, 687 (1959)